Title
Ionomer Optimization for Hydroxide-Exchange-Membrane Water Electrolyzers Operated with Distilled Water: A Modeling Study

Journal
Journal of The Electrochemical Society, 169(5)

ISSN
0013-4651

Authors
Liu, Jiangjin
Weber, Adam Z

Publication Date
2022-05-01

DOI
10.1149/1945-7111/ac69c4

Peer reviewed

Ionomer Optimization for Hydroxide-Exchange-Membrane Water Electrolyzers Operated with Distilled Water: A Modeling Study

Journal of The Electrochemical Society, 2022 **169** 054506

Ionomer Optimization for Hydroxide-Exchange-Membrane Water Electrolyzers Operated with Distilled Water: A Modeling Study

Jiangjin Liu and Adam Z. Weber[*,z]

Energy Conversion Group, Lawrence Berkeley National Laboratory, Berkeley, California 94720, United States of America

The hydroxide-exchange-membrane water electrolyzer (HEMWE) is a promising means to store intermittent renewable energy in the form of hydrogen chemical energy. The hydroxide-exchange ionomer (HEI) in the gas-evolving electrodes and the hydroxide-exchange membrane (HEM) are key components of HEMWE. In this work, we simulate the cell and examine explicitly the impact of HEI and HEM properties with a focus on improving HEMWE performance when operated with distilled water (*i.e.*, no supporting electrolyte). The tradeoff between the ionic conductivity gain and electrochemically active surface area (ECSA) loss is studied. For a constant catalyst loading, distributing more catalyst next to the HEM or making thinner but denser catalyst layer is beneficial for HEMWE performance. The results demonstrate that a higher water diffusion coefficient is desired for HEM to supply reactant water to the cathode. In contrast, a lower water diffusion coefficient is preferred for the cathode HEI to retain the water in the regions with high reaction rates. Overall, the findings provide important insights to optimizing HEI/HEM materials for improved HEMWE performance.

 [DOI: 10.1149/1945-7111/ac69c4]

Manuscript submitted February 18, 2022; revised manuscript received April 5, 2022. Published May 4, 2022. *This paper is part of the JES Focus Issue on Advanced Electrolysis for Renewable Energy Storage.*

Supplementary material for this article is available online

Nomenclature

Abbreviations

aPTL	Anode porous transport layer
aCL	Anode catalyst layer
HEI	Anion exchange ionomer
HEM	Anion exchange membrane
HEMWE	Anion exchange membrane water electrolzyer
cCL	Cathode catalyst layer
CL	Catalyst layer
cPTL	Cathode porous transport layer
HER	Hydrogen evolution reaction
OER	Oxygen evolution reaction

List of Symbols

a	ECSA (m^2)
a_0	Entire ECSA (m^2)
a_{eff}	Effectively utilized ECSA (m^2)
$a^{specifc}$	Specific ECSA ($1\ m^{-1}$)
a_{H_2O}	Water activity
c_i	Concentration of species i ($mol\ m^{-3}$)
D	Diffusion coefficient ($m^2\ s^{-1}$)
F	Faraday's constant ($C\ mol^{-1}$)
H	Enthalpy ($J\ kg^{-1}$)
i_0	Exchange current density ($A\ m^{-2}$)
i_{cell}	Cell current density ($A\ m^{-2}$)
i_{rxn}	Volumetric reaction current ($A\ m^{-3}$)
k	Rate coefficients of reactions and phase changes ($1\ s^{-1}$)
k_α	Permeability of phase α (m^2)
k_{thru}	Coefficient for breakthrough liquid flux ($kg\ (m^2{\cdot}s)^{-1}$)
k_T	Thermal conductivity ($W\ (m{\cdot}K)^{-1}$)
M	Molar mass ($g\ mol^{-1}$)
n	Outward unit vector at the PTL/channel boundary
$\boldsymbol{N}$	Flux vector ($mol\ m^{-2} \cdot s^{-1}$)
p	Pressure (Pa)
Q	Heat source ($W\ m^{-3}$)
R	universal gas constant ($J\ (mol{\cdot}K)^{-1}$)
R_{rxn}	Mass source term from reactions ($kg\ (m^3 \cdot s)^{-1}$)
R_{phase}	Mass source term from phase change ($kg\ (m^3 \cdot s)^{-1}$)
T	Temperature (K)
U_0	Equilibrium potential (V)
v	Velocity ($m\ s^{-1}$)
$\bar{V}_{H_2O,L}$	Molar volume of liquid water ($m^3\ mol^{-1}$)
x	Molar fraction of gas species
z	Charge number

Greek Symbols

α	Symmetry coefficient
α_W	Water diffusion coefficient ($mol^2\ (J{\cdot}m{\cdot}s)^{-1}$)
θ	Bubble coverage
κ	Ionic conductivity ($S\ m^{-1}$)
η	Overpotential (V)
σ	Electronic conductivity ($S\ m^{-1}$)
ϵ	Porosity
ϵ_α	Volume fraction of phase α
ξ	Electroosmosis coefficient
λ	Water content in ionomer phase
μ_α	Dynamic viscosity of phase α (Pa·s)
μ_{H_2O}	Water chemical potential ($J\ mol^{-1}$)
ρ	Density ($kg\ m^{-3}$)
τ	Tortuosity factor
ϕ_1	Electronic potential (V)
ϕ_2	Ionic potential in ionomer (V)
ω	Mass fraction

Superscripts and subscripts

a	Anodic
c	Cathodic
eff	Volume averaged effective property
ev	Evaporation
gen	Generation
G	Gas phase
i	Gas species i

*Electrochemical Society Fellow.
[z]E-mail: azweber@lbl.gov

L	Liquid phase
M	Ionomer/membrane phase
res	Residual
rxn	Reaction
sat	Saturation/saturated
t	Triple point property
thru	Breakthrough
V	Vapor phase

Hydrogen is a vital material that features high specific energy density and broad industrial applications.[1–3] Today, hydrogen is still predominantly produced via steam methane reforming, which has high carbon dioxide emissions. With the more stringent environment requirements and ever increasing energy demand, more environmentally friendly and efficient ways of hydrogen production are needed.[4–7] Low temperature water electrolysis can transform the intermittent renewable energy sources like wind and solar energy into the chemical energy of hydrogen, thus producing hydrogen in a clean and sustainable way.[8,9] Hydroxide-exchange-membrane water electrolyzer (HEMWE) is a promising low-temperature water-electrolysis technique.[10,11] Like the proton-exchange-membrane (PEM) water electrolyzers, it can produce pressurized hydrogen without extra mechanical compression and in a small form factor. In addition, unlike PEMWE, HEMWE can utilized non platinum-group-metal catalysts due to the alkaline environment, similar to traditional liquid-alkaline water electrolysis.[12–15]

Figure 1 shows a schematic of the components, the transport, and the electrochemical reactions of a HEMWE. The hydroxide-exchange-membrane (HEM) electronically isolates the anode and cathode but allows passage of hydroxide ions between them. Each electrode consists of catalyst layer (CL), porous transport layer (PTL), and bipolar plate (BPP). With energy supplied, water splits into oxygen and hydrogen via the oxygen evolution reaction (OER) at the anode and hydrogen evolution reaction (HER) at the cathode, respectively. The hydroxide ions are driven by potential difference from cathode to anode through the HEM. Water is transported both by diffusion down its chemical potential gradient as well as by electroosmosis due to the hydroxide ion migration.

The development of the HEMWE is still at early stages featured by sporadic reports from mostly academic groups focusing on developing new materials, especially for hydroxide-exchange ionomer (HEI) and HEM.[10,11,16–21] Though HEI/HEM has been studied within the context of HEM fuel cells,[22–26] the environment in HEMWE is different, which requires different optimization criteria for the HEI/HEM. Mathematical modeling is a time and cost efficient approach towards deconvoluting the underlying physics and understanding the complex transport and reaction processes within the cell and components so as to elucidate the limiting phenomena in the cells. Such analysis provides targets for material properties and guides the design and integration of them into cells. However, cell-level models that can explore the complex multi-phase transport in the HEMWEs and their impact on the cell performance are still lacking in the literature. An et al.[27] developed a 1D mathematical model to study the impact of membrane thickness and exchange current densities. However, the coupled ion and water transport in the ionomer phase were not explicitly modeled and the CLs are only considered as interfaces.

We previously developed a mathematical model to elucidate the functionality of the supporting liquid electrolyte, i.e., KOH solution.[28] In this work, we extend our model to study the desired properties of the HEI/HEM for HEMWE operating with distilled (DI) water through examining key transport mechanisms, local distributions, and applied-voltage-breakdowns. This article is organized as follows. First, the model is presented with detailed discussion of the physics and parameters. Then the model is validated and applied to identify the key properties of HEI in the gas-evolving electrodes and those of the HEM. The different material requirements for HEMWEs operated with DI water and liquid electrolytes (KOH solution) are discussed, and the local distributions and the applied-voltage-breakdowns are presented.

Methods

Mathematical modeling.—The 1-D, continuum, two-phase HEMWE model is extended from our previous work.[28,29] Steady-state operation and thermal equilibrium between different phases are assumed. The model domains include the hydroxide-exchange-membrane (HEM), anode catalyst layer (aCL), anode porous transport layer (aPTL), cathode catalyst layer (cCL) and cathode porous transport layer (cPTL). The baseline model dimensions, materials and physical properties are summarized in Table SI. Details of the governing equations are discussed in the following sections with various symbols listed in the nomenclature table. The

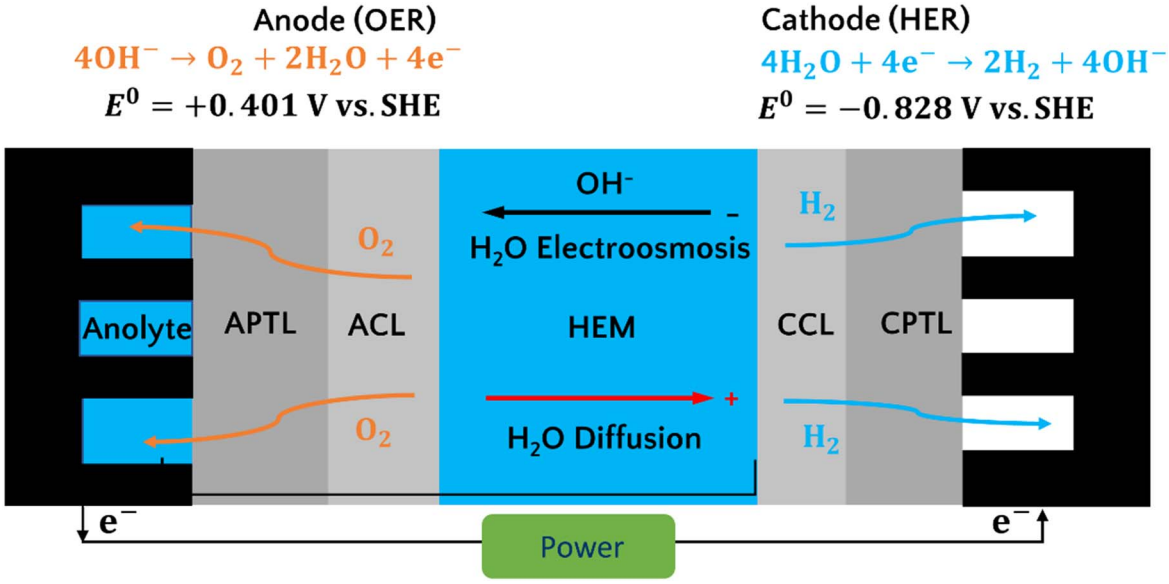

Figure 1. Schematic of an HEMWE. It consists of anode porous transport layer (aPTL), anode catalyst layer (aCL), hydroxide-exchange-membrane (HEM), cathode catalyst layer (cCL), cathode porous transport layer (cPTL) and bipolar plates (BPP). Oxygen evolution occurs at the anode and hydrogen evolution occurs at the cathode. Hydroxide ions transport from cathode to anode and water transport from the liquid water anode to drier cathode through the HEM.

additional physics considering the effects of the liquid electrolyte are summarized in SI.[28]

Gas mixture and liquid transport.—Both gas mixture and liquid transport in the porous media (CLs and PTLs) are studied by mass conservation and Darcy's law

$$\nabla\cdot\left(-\frac{\rho_\alpha k_\alpha^{eff}}{\mu_\alpha}\nabla p_\alpha\right) = R_{rxn,\alpha} + R_{phase,\alpha} \quad [1]$$

where ρ_α, k_α^{eff}, μ_α and p_α are the density, effective permeability, dynamic viscosity, and pressure of phase α, respectively. $R_{rxn,\alpha}$ and $R_{phase,\alpha}$ account for the sources from reactions and water phase change, respectively. The water phase change term is further discussed below. The source terms in each domain are summarized in Table SII. The operating pressure is specified at the PTL/channel interface, i.e., the outside boundary of PTL. For an electrode fed with liquid, the liquid pressure is set to 1 atm at the PTL/channel interface. For an electrode without feeding liquid, a mass flux is set following the approach of Zhou et al.[30]

$$-\left(\frac{\rho_L k_L^{eff}}{\mu_L}\nabla p_L\right)\cdot\mathbf{n} = k_{thru}\frac{p_L - p_{L,\text{break}}}{1\ [\text{Pa}]}\left[1 + \tanh\left(\frac{p_L - p_{L,\text{break}}}{1\ [\text{Pa}]}\right)\right] \quad [2]$$

where $\mathbf{n}$ is the outward unit vector at the PTL/channel boundary and $p_{L,\text{break}}$ is the liquid breakthrough pressure required at the PTL/channel interface and is set as 2 kPa in this work. The coefficient k_{thru} is set as 0.1 kg $(\text{m}^2\cdot\text{s})^{-1}$.

Molecular diffusion.—Gas diffusion is modeled by species mass conservation and Stefan-Maxwell equations,

$$\nabla\cdot\left(-\rho_G\omega_i\sum_j^n \bar{D}_{ij}^{eff}(\nabla x_j + (x_j-\omega_j)\nabla p_G/p_G)\right) + \rho_G(\boldsymbol{v}\cdot\nabla)\omega_i = R_{rxn,\omega_i} + R_{phase,\omega_i} \quad [3]$$

where ω_i and x_i are mass and molar fractions of gas species i, respectively, $\boldsymbol{v}$ is the gas-mixture velocity, and the effective diffusion coefficient, $\bar{D}_{ij}^{eff}$, is calculated from

$$\bar{D}_{ij}^{eff} = \frac{\epsilon_G}{\tau_G}\bar{D}_{ij} \quad [4]$$

where ϵ_G and τ_G are the volume fraction and tortuosity factor of the gas phase, respectively. The binary diffusion coefficient $\bar{D}_{ij}$ is dependent on the gas-mixture composition.[31] Gas composition and relative humidity (RH) are specified at the PTL/channel interface as boundary conditions.

Electron conduction.—Electron transport is modeled by charge conservation and Ohm's law

$$\nabla\cdot(-\sigma^{eff}\nabla\phi_1) = -i_{rxn} \quad [5]$$

where σ^{eff} is the effective electronic conductivity and ϕ_1 is the electronic potential. i_{rxn} is the local volumetric reaction current as discussed below. Cell operating potential and an arbitrary zero potential are set at the anode and cathode BPP, respectively.

Ion transport in ionomer and membrane.—Ion transport in the ionomer phase (membrane and catalyst layer) is described by

$$N_{OH^-} = -\frac{\kappa_{OH^-}}{z_{OH^-}F}\nabla\phi_2 - \frac{\xi_{OH^-}\kappa_{OH^-}}{z_{OH^-}^2F^2}\nabla\mu_{H_2O,M} \quad [6]$$

where κ_{OH^-}, z_{OH^-} and ξ_{OH^-} are the ionic conductivity, charge number and electroosmotic coefficient of OH^-, respectively. F is Faraday's constant. The two transport mechanisms are migration driven by ionic potential in the ionomer phase, ϕ_2 and streaming current driven by water chemical potential, $\mu_{H_2O,M}$. No flux boundary conditions are set at the CL/PTL interfaces.

Mass conservation is applied for OH^-

$$\nabla\cdot\boldsymbol{N}_{OH^-} = -\frac{i_{\text{rxn}}}{F} \quad [7]$$

Water transport in ionomer and membrane.—Figure 1 shows the schematic of the water transport in the ionomer phase. With only a liquid water feed to the anode, water diffuses from anode to cathode to supply the reactant water and hydrates the HEM and the cCL HEI. On the other hand, electroosmosis transports water from the cathode to anode moving with the hydroxide flux. Water transport is described by

$$N_{H_2O,M} = -\left(\frac{\kappa_{OH^-}^{eff}\xi_{OH^-}}{z_{OH^-}F}\right)\nabla\phi_2 - \left(\alpha_W + \frac{\kappa_{OH^-}^{eff}\xi_{OH^-}^2}{z_{OH^-}^2F^2}\right)\nabla\mu_{H_2O,M} \quad [8]$$

with mass conservation given by

$$\nabla\cdot\boldsymbol{N}_{H_2O,M} = R_{H_2O,\text{gen}} + R_{L,M} + R_{V,M} \quad [9]$$

The water production rate in anode is

$$R_{H_2O,\text{gen}} = \frac{i_{rxn}}{2F} \quad [10]$$

and that in the cathode is

$$R_{H_2O,\text{gen}} = -\frac{i_{rxn}}{F} \quad [11]$$

The water absorption or desorption from the ionomer phase into the liquid and vapor phase along with the water evaporation are described in detail in the next section.

Water phase-change.—There are three phases of water considered in the model: water absorbed in the ionomer phase, liquid water, and water vapor. The water phase-change rates between them are calculated based on the chemical potentials in each phase. The chemical potential of ionomer absorbed water $\mu_{H_2O,M}$ is solved from the water transport in the ionomer phase as described above (Eqs. 8–11). The water chemical potential in liquid and vapor phases are functions of gas and liquid pressures and temperatures relative to those at the triple point

$$\mu_{H_2O,L} = H_{H_2O,L}M_{H_2O}\left(1 - \frac{T}{T_t}\right) + C_{p,H_2O,L}M_{H_2O}\left(T - T_t - T\ln\left(\frac{T}{T_t}\right)\right) + \bar{V}_{H_2O,L}(P_L - P_t) \quad [12]$$

$$\mu_{H_2O,V} = H_{H_2O,V}M_{H_2O}\left(1 - \frac{T}{T_t}\right) + C_{p,H_2O,V}M_{H_2O}\left(T - T_t - T\ln\left(\frac{T}{T_t}\right)\right) + RT\ln\left(\frac{p_{H_2O,V}}{p_t}\right) \quad [13]$$

R is universal gas constant. The thermodynamic properties in the Eqs. 12 and 13 are summarized in Table SIII. The water evaporation rate is calculated as

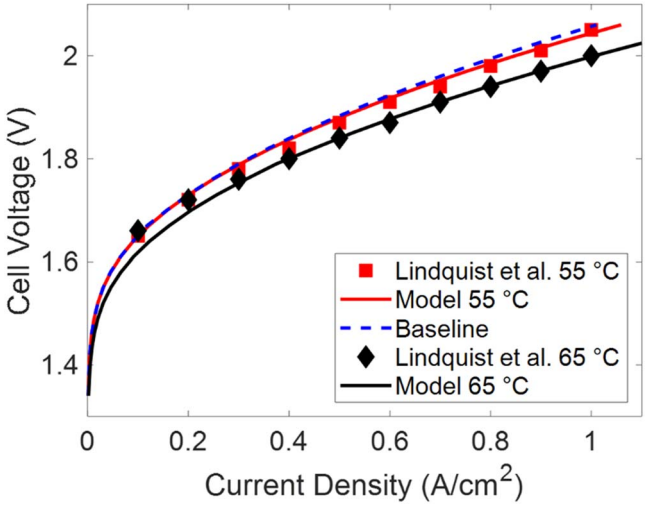

Figure 2. Model validation by comparing with the polarization curves from Lindquist et al.[40] The baseline cell with vapor cathode (100% RH) shows almost identical performance with the cell operated with water fed to both electrodes.

$$R_{L,V} = \begin{cases} \frac{k_{ev}}{M_{H_2O}}(\mu_{H_2O,L} - \mu_{H_2O,V}) & \text{if } \mu_{H_2O,V} > \mu_{H_2O,L} \text{ (i.e., saturated vapor)} \\ \frac{k_{ev}}{M_{H_2O}}(\mu_{H_2O,L} - \mu_{H_2O,V})(S_L - S_{L,res}) \end{cases} \quad [14]$$

where S_L and $S_{L,res}$ are the liquid saturation and residual liquid saturation in the porous media, respectively. The saturation is determined by interpolation functions of the water-retention curves, which plot the liquid water saturation as a function of the capillary pressure $p_C = p_L - p_G$.[32,33] A negative $R_{L,V}$ indicates water condensation instead of evaporation. The water absorption from liquid into ionomer phase is calculated as

$$R_{L,M} = \begin{cases} \frac{k_{ad,M,L}}{M_{H_2O}}(\mu_{H_2O,L} - \mu_{H_2O,M}) & \text{if } p_L > 0 \text{ (i.e., there is liquid)} \\ 0 \end{cases} \quad [15]$$

The water absorption from vapor into ionomer phase is calculated as

$$R_{M,V} = \frac{k_{ad,M,V}}{M_{H_2O}} \exp(4.48 a_{H_2O,M})(\mu_{H_2O,V} - \mu_{H_2O,M}) \quad [16]$$

The exponential dependence on local water activity $a_{H_2O,M}$ is adopted from Kientiz et al.,[34] which is valid for PEMs and assumed the same as HEM. The water activity is a function of the chemical potential of the water in ionomer phase

$$a_{H_2O,M} = \frac{p_t}{p_{H_2O,sat}} \exp\left(\frac{\mu_{H_2O,M} - H_{H_2O,V} M_{H_2O}\left(1 - \frac{T}{T_t}\right) - C_{p,H_2O,V} M_{H_2O}\left(T - T_t - T \ln\left(\frac{T}{T_t}\right)\right)}{RT}\right) \quad [17]$$

where $p_{H_2O,sat}$ is the water vapor saturation pressure, and the other terms are defined in Table SIII. The water content λ, which is defined as the number of water molecules per charged group, is a function of the water activity,[35,36]

$$\lambda = (-0.6 a_{H_2O,M}^3 + 0.85 a_{H_2O,M}^2 - 0.2 a_{H_2O,M} + 0.153)(T - 313) + 39 a_{H_2O,M}^3 - 47.7 a_{H_2O,M}^2 + 23.4 a_{H_2O,M} + 0.117 \quad [18]$$

A maximum of $\lambda_{max} = 19$ is set at full liquid equilibration.

Energy transport.—Temperature (T) is governed by Fourier's law and conservation of energy

$$\nabla \cdot (-k_T^{eff} \nabla T) = Q_{gen} \quad [19]$$

where k_T^{eff} is effective thermal conductivity. The involved source terms (Q_{gen}) in each modeling domain are specified in Table SII. The operating temperature is specified at the PTL/channel interface as the boundary condition.

Electrochemical reactions.—OER.—Hydroxide is electrochemically oxidized to evolve oxygen in the anode as shown in Fig. 1. The OER kinetics is modeled with Tafel equation

$$i_{rxn}^{OER} = a_{OER}^{specific} i_0^{OER} \exp\left(\frac{\alpha_{OER} F}{RT} \eta\right) \quad [20]$$

where the specific electrochemically active surface area (ECSA), $a^{specific}$, is the active catalyst surface area per unit volume of the catalyst layer. i_0^{OER} is the exchange current density,[28,37] α_{OER} is the transfer coefficient, and η is the overpotential

$$\eta = \phi_1 - \phi_2 - U_0 \quad [21]$$

where U_0 is the equilibrium potential.HER.—Water is reduced to form hydrogen in the cathode as shown in Fig. 1. The HER kinetics is modeled by Butler-Volmer equation[28,37]

$$i_{rxn}^{HER} = a_{HER}^{specific} i_0^{HER} a_{H_2O,M} \left[\exp\left(\frac{\alpha_{HER,a} F}{RT} \eta\right) - \exp\left(-\frac{\alpha_{HER,c} F}{RT} \eta\right)\right] \quad [22]$$

The subscript a and c denote anodic and cathodic, respectively. Bubble coverage.—An empirical relationship between the fractional bubble coverage and the cell current density is implemented into the model to calculate the ECSA loss due to gas bubble coverage.[38]

$$\theta = 0.023\left(\frac{i_{cell}}{\text{Am}^{-2}}\right)^{0.3} \quad [23]$$

where i_{cell} is the superficial current density of the HEM electrolyzer. The catalyst surface covered by the bubbles are assumed to be turned off for reactions. Then the effective ECSA is calculated as

$$a_{eff} = a_0(1 - \theta) \quad [24]$$

where a_0 is the entire ECSA and a_{eff} is the effectively utilized ECSA which are not covered by bubbles.

Applied-voltage breakdown (AVB).—We apply the power-loss post-processing method to breakdown the voltage losses in the HEMWE.[39] The overall overpotential is decomposed into the anode kinetics loss, cathode kinetics loss, high-frequency resistance (HFR) loss, anode ohmic loss and cathode ohmic loss. The mathematical expressions for each type of voltage loss are described in the **SI**.

Results and Discussion

Model validation.—Due to the lack of broadly accessible commercial materials and inconsistencies in cell preparation,

HEMWE performance widely varies,[10,11] especially with DI water feeds. To validate the model, the data from Lindquist et al.[40] is used as it is some of the highest and reproducible HEMWE performance with DI water and baseline materials and operation; detailed information of the cell configuration is summarized in Table SI. Model and data comparison is compared in Fig. 2. The model was first calibrated at 55 °C and matches well at both 55 °C and 65 °C with the experimental data for both small and large current densities.

In Lindquist et al.,[40] liquid water is fed to both electrodes. To ease mode of operation, HEMWE is usually operated with vapor cathode, i.e., liquid water is only fed to the anode. To examine this, we simulated a cell with a vapor cathode, where 100% RH is maintained in cathode. Almost identical performance is achieved as the cell with liquid water on both electrodes (Fig. 2); we refer to this 100% RH vapor cathode cell as the baseline cell. However, when the cathode RH is low, the reactant water relies on water transport from anode to cathode and water management may become a concern.

Anode-catalyst-layer hydroxide-exchange ionomer.— *Tradeoff between the ionic conductivity and water swelling.*—The HEI serves two main purposes. First, it contributes to ion delivery from the HEM to the reaction sites in the catalyst layers. Second, it serves as binder to adhere the catalyst together and with adjacent layers. The importance of HEI in ion conduction depends on the liquid electrolyte fed into the HEMWE. Figure 3a compares the impact of ionomer ionic conductivity on the performance of the cells with DI water and 1 M KOH solution. The baseline model with DI water has a current density of 1 A cm^{-2} at 2.06 V. By feeding 1 M KOH solution to the cell, the performance is improved, and it reaches 1 A cm^{-2} at a lower voltage of 1.78 V. Next, the ionomer conductivity is varied from these baseline values. For the same anode ionomer conductivity loss, there is a larger loss in current density of the DI water cell. For example, with 90% ionic conductivity loss, only half of the DI water cell current density is realized, while the KOH cell still maintains a high current density of 0.81 A cm^{-2}. The difference is even larger at lower ionic conductivities. As expected, with almost no ionic conductivity in the HEI, the DI water cell can hardly operate as ions cannot reach the reaction sites effectively. In contrast, the KOH cell still has a current density of 0.43 A cm^{-2} as ions can still transport through the liquid electrolyte in the CL. High ion-exchange-capacity (IEC) ionomers have higher ionic conductivity but also higher water uptake and swelling, which can result in catalyst detachment and ECSA loss. Figure 3b further studies the tradeoff between the ionic conductivity gain and ECSA loss in a cell with DI water. A negative ECSA loss indicates increased ECSA. The conductivity increase as a function of the ECSA loss is calculated by changing the aCL HEI conductivity for different ECSA values in order to maintain the baseline performance of 1 A cm^{-2} at 2.06 V. We can see from Fig. 3b that higher aCL HEI conductivity can compensate for the decrease in ECSA and higher OER kinetic loss (see Fig. S1 (available online at stacks.iop.org/JES/169/054506/mmedia)). The higher aCL HEI conductivity results in lower aCL ohmic losses and it also helps to access more of the catalyst sites deeper (further from the membrane as shown in Fig. S1) in the aCL, thus increasing aCL utilization. The increase in aCL HEI conductivity exhibits an exponential relationship based on ECSA loss. When ECSA variation is not that large, a moderate conductivity change is sufficient to maintain the same performance. However, when ECSA loss approaches 50%, the ionic conductivity needs to be doubled to compensate for the loss. On the other hand, even if there is a large ECSA increase (ECSA loss $= -50\%$), the ionic conductivity cannot decrease too much ($< 30\%$) to keep the same cell performance. This nonlinear relationship is because the ion conduction relies solely on the HEI when the cell is operated with DI water and a minimum level of ionic conductivity is necessary to deliver ions to the reaction sites. The shaded region in Fig. 3b indicates the ionomer with preferred properties when considering the tradeoff between conductivity gain and ECSA loss.

ECSA distribution and aCL thickness.—Due to inhomogeneity in the fabrication process or degradation issues, the catalysts can be nonuniformly distributed in the aCL. We applied the mathematical model to study the impact from the nonuniform ECSA through the thickness of the aCL. Three cases with different ECSA distribution were examined (inset in Fig. 4a). Case 1 has uniform ECSA through the aCL thickness. Case 2 and 3 follow parabolic distributions with more ECSA next to the HEM in case 2 and more ECSA next to the CL/PTL interface in case 3. The total ECSA is kept constant for all the three cases. Case 2 has more ECSA next to HEM, which reduces the ion transport distance to reach the reaction sites, and thus reduces the aCL ohmic loss (Fig. 4b), thereby resulting in the highest performance. However, case 2 might have issues with bubble removal as it has higher reaction currents next to the HEM and the bubbles generated there must transport through the whole CL to be removed. In case 3**,** the ion-rich region next to the HEM has small ECSA, which shows as a slightly extended kinetic region in the polarization curve since the highest ECSA is further from the ion source. Therefore, unlike case 1 and 2 that exhibit higher reaction current densities next to the HEM, the distribution of reaction current density in case 3 is more complex as the reaction can be limited by either ECSA and/or ion transport (Fig. S2). As a result, case 3 exhibits higher aCL ohmic loss and anode kinetics loss (Fig. 4b). One benefit of the more uniformly distributed reaction current is more moderate local bubble coverages. From the results,

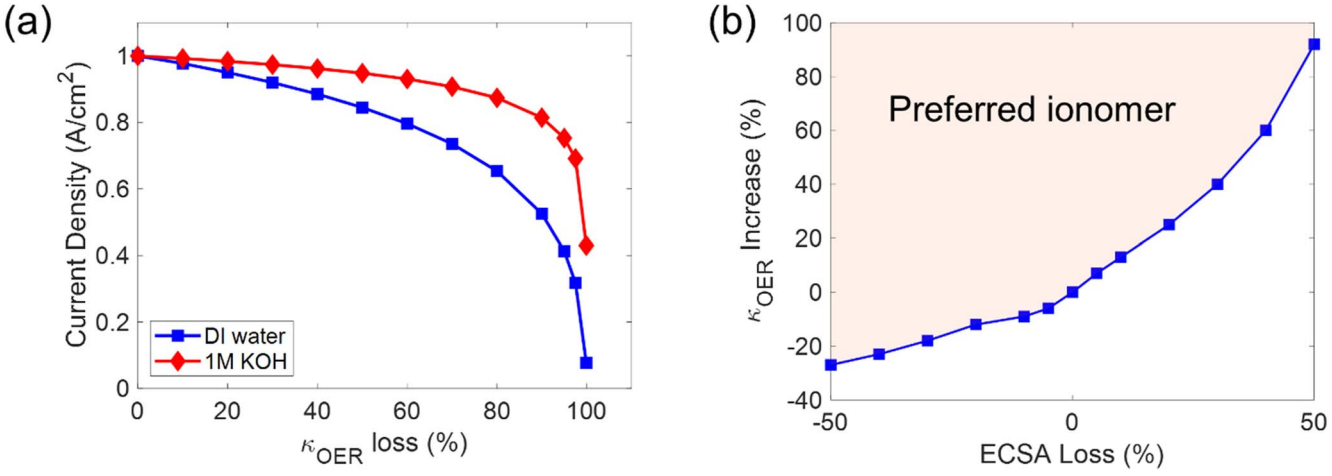

Figure 3. (a) Comparison of the current density variations as a function of the anode HEI ionic conductivity (κ_{OER}) loss in the cells fed with DI water and 1 M KOH. The cell voltages are 2.06 V and 1.78 V for the DI water cell and 1 M KOH cell, respectively. (b) The tradeoff between the ionic conductivity and ECSA for the cells operated with DI water.

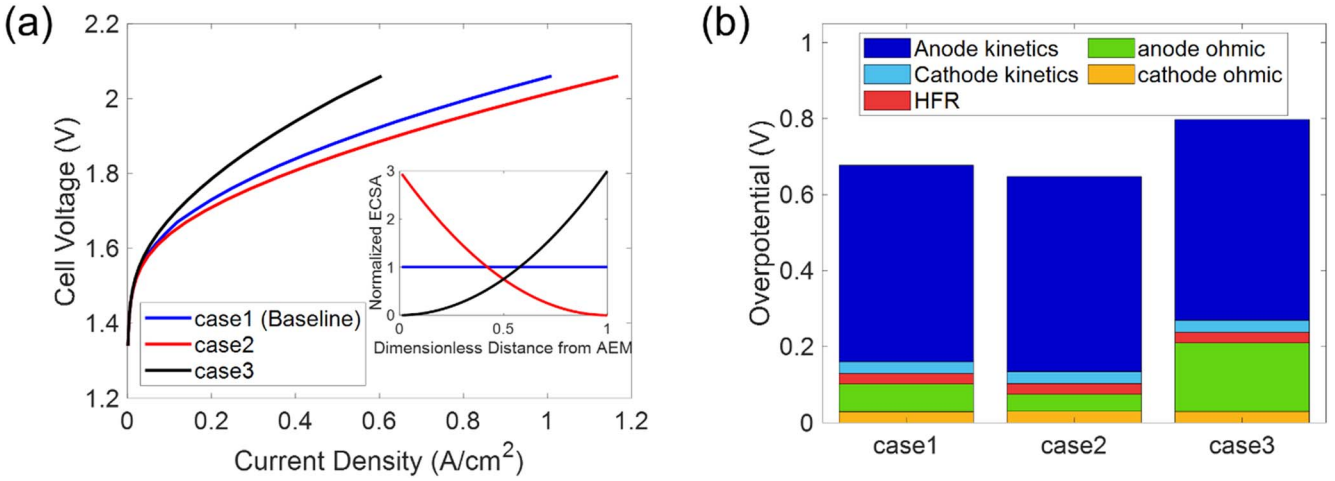

Figure 4. ECSA gradient analysis. (a) Polarization curves for the 3 cases with the inset showing the normalized ECSA distribution. (b) Applied-voltage breakdown at a cell current density of 0.5 A cm^{-2} for the 3 cases.

one option for optimizing the CL structure is to deposit more catalyst in the region next to the HEM. Another inference from the above analysis is to make thinner but denser OER electrode to reduce the overall ion transport length and thus ohmic losses. The cell with half-thickness but the same total ECSA exhibitsbetter performance (Fig. S3) due to the shortened ion-transport length needed to reach the reaction sites, resulting in lower aCL ohmic and kinetic losses.

Hydroxide-exchange-membrane.—The HEM is a key component for ion and water transport between the anode and cathode and optimizing its conductivity and water-transport properties is crucial for improving cell performance.

Water transport (diffusion and electroosmosis).—Reactant water in the cathode relies on water transport from anode to cathode when the cell is operated with a low RH vapor cathode. As shown in Fig. 5a, reducing the cathode RH from baseline (100%RH) to 30% RH decreases the performance due to dehydration of the HEM and cCL. Figure 6a shows the cathode ionomer water content, which is defined as the number of water molecules per charged group. While at baseline (100%RH), the whole cCL is hydrated well, the water content in the 30% RH cell is lower and decreases from the HEM to PTL. The lower reactant water activity in the cathode results in higher cathode kinetics and ohmic losses (see Fig. 5b), indicating nonsufficient reactant water supply to the cathode.

Water diffuses from anode to cathode and is transported from cathode to anode by electroosmosis. Thus, the overall water movement in the HEMWE can be adjusted by tuning the HEM water-transport properties. Figure 5a shows the polarization curves of the 30% RH cell with modified water-transport properties. Decreasing the water diffusion coefficient results in worse performance due to the much higher cathode kinetics loss and cathode and HFR ohmic losses (Figs. 5b and S4). It also makes the reaction current more concentrated next to the HEM and reduces the CCL utilization (Fig. 6b). Increasing the water diffusion coefficient improves the performance as it facilitates water movement from anode to cathode and results in better HEM and cCL HEI hydration (Fig. 6a). This result is consistent with the experimental observations in Chen et al., which emphasizes the importance of high HEM water diffusivity.[18] Kiessling et al. also reported hydration issues at high current densities in the drier cathode, though they operated the cell with alkaline solutions in the anode.[41] In contrast, increasing the electro-osmotic coefficient results in further cathode dehydration (Fig. 6a) and thus worse performance due to higher cathode kinetics and ohmic losses (see Fig. 5b).

Ionic conductivity and thickness.—Figure S5 shows that either increasing the HEM ionic conductivity or reducing the HEM thickness results in better performance. The cell with half-thick HEM performs slightly better than the cell with doubled HEM ionic

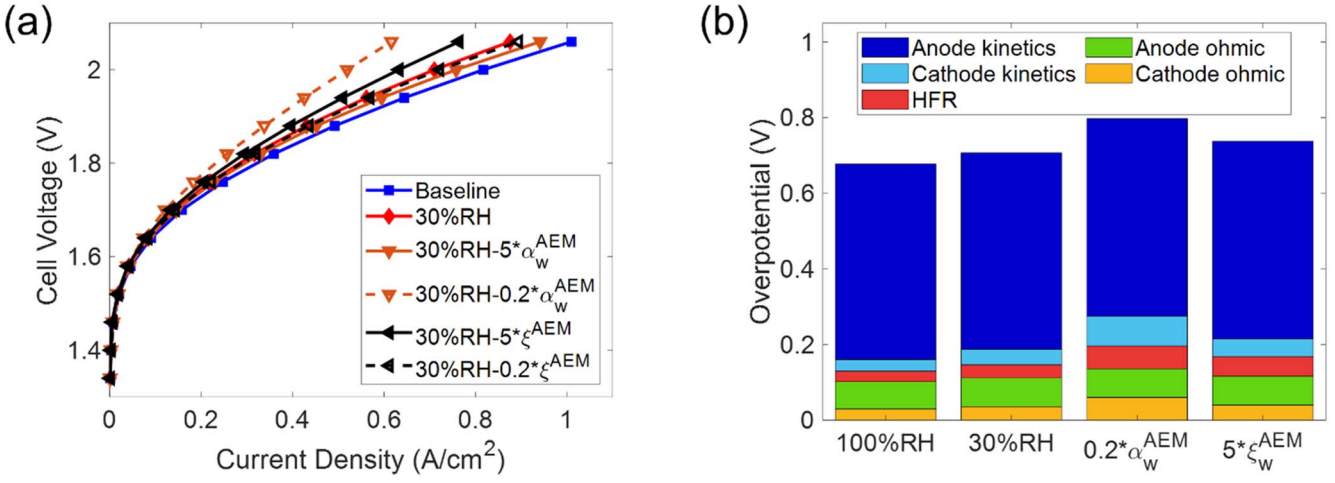

Figure 5. (a) Cell polarization curves and (b) applied-voltage breakdown at a cell current density of 0.5 A cm^{-2} for the baseline cell (100% RH in cathode) and the 30% RH cell with modified HEM water diffusion coefficients or electroosmotic coefficients.

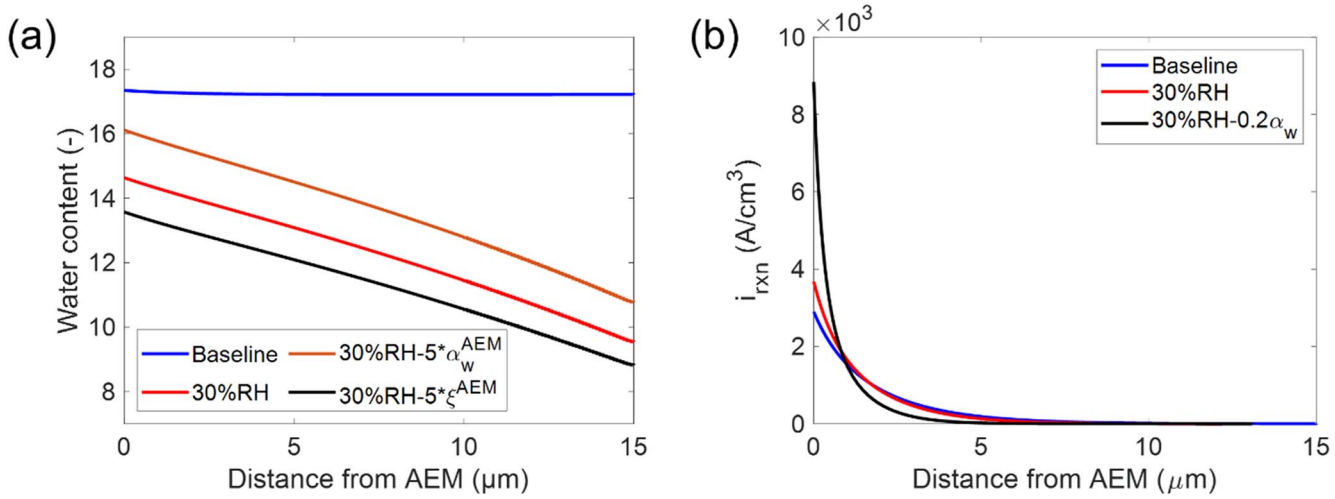

Figure 6. The (a) water content and (b) reaction current density distributions in the cCL for the baseline cell (100% RH in cathode) and the 30% RH cell with modified HEM water diffusion coefficients or electroosmotic coefficients.

conductivity as it not only reduces HEM ohmic loss but also improves water transport from anode to cathode. Thus, there is not a perfect correlation in terms of conductivity, thickness, and area specific resistance due to the changes in water management and hydration. However, thinning the HEM might result in crossover or mechanical stability issues, which are not considered in current model but could result in failures in practical cells.

Cathode-catalyst-layer hydroxide-exchange ionomer.— *Water transport.*—The impact from the cCL HEI water-transport properties is different from that of the HEM. Decreasing the water diffusion coefficient results in better performance (Fig. 7a). This might be counterintuitive as water is a reactant in the cathode and thus improving the water movement is expected to improve the performance. As shown in Fig. 8a, though the average water content is slightly lower in the cell with lower water diffusion coefficient, it exhibits a larger water content gradient and higher water content in the region next to HEM. The region next to the HEM has higher ionic potentials and thus higher reaction rates. Increasing the reactant water activity in this region reduces the cathode kinetics loss and slightly reduces the cCL ohmic loss due to the shortened ion-conduction path (Fig. 7b). Figure 8b shows the water vapor partial pressure in cCL and cPTL. The outside boundary of the cPTL has the same water vapor partial pressure due to the same operating RH and gas pressure. Overall, the water in the cathode is supplied from the anode and leaves the cell through the cPTL. Lowering the water diffusion coefficient in cathode results in much lower average water vapor partial pressure in the cCL and cPTL. However, like the water content in the cCL, the gradient of water vapor partial pressure is larger due to the lower transport properties, resulting in a higher partial pressure in the region next to the HEM. The qualitative illustration of the overall water activity distribution in the HEM and cathode is shown in Fig. S6, where the drier cathode obtains water from the anode through the HEM, and a lower water diffusion coefficient in the cathode ionomer helps to retain more water in the region next to the HEM where HER predominantly occurs. Thus, though the average cathode water content and water-vapor partial pressure are lower, the cell with lower water diffusion coefficient demonstrates better performance.

HEI conductivity.—For the vapor cathode cells, water swelling, and the resultant catalyst detachment issues, are not significant. Thus, a high IEC ionomer is expected to improve the performance. As shown in Fig. 7a, by increasing the cCL HEI conductivity, the cell performance is predicted to improve, which is consistent with the experimental results in Huang et al.[21] The AVB in Fig. 7b shows that cathode kinetics and ohmic losses are reduced in the cell with higher cathode ionomer conductivity.

Conclusions

In this work, we applied a multiphysics mathematical model to study the optimized properties of the hydroxide-exchange ionomer

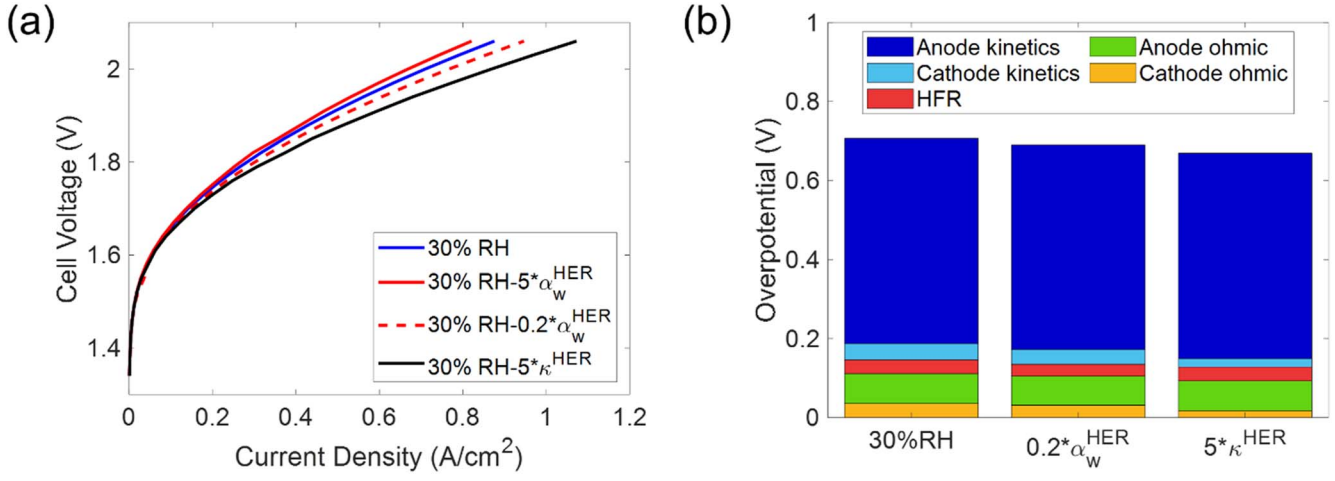

Figure 7. The (a) polarization curves and (b) applied-voltage breakdown at a cell current density of 0.5 A cm^{-2} for cells with different cCL HEI properties.

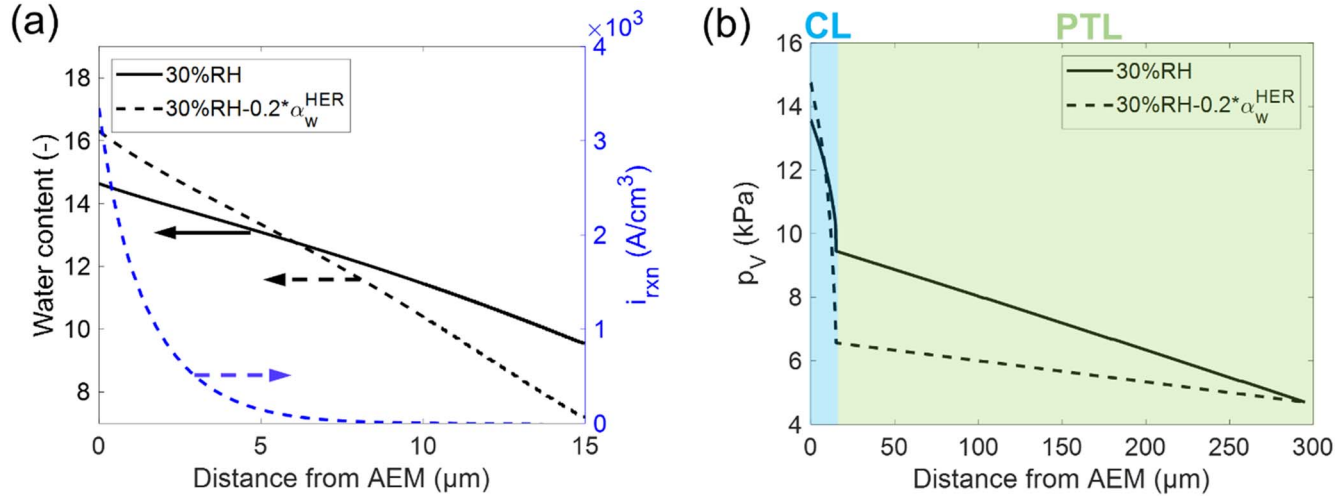

Figure 8. (a) Water content and reaction current density distributions in the cCL. (b) Water vapor partial pressure in the cCL and cPTL at a cell current density of 0.5 A cm^{-2} for cells with different cCL HEI properties.

(HEI) and hydroxide-exchange membrane (HEM) for hydroxide-exchange-membrane water electrolyzers (HEMWEs). The tradeoff analysis between the ionic conductivity gain and electrochemically active surface area (ECSA) loss shows that the ionic conductivity of anode HEI is critical for HEMWE operated with DI water as it solely relies on the HEI for ion delivery to the reaction sites in contrast to cells operated with alkaline solutions. For cells with a constant catalyst loading, distributing more ECSA next to the HEM or making denser but thinner anode catalyst layers improves the performance by reducing the anode ohmic and kinetics losses. Increasing the water diffusion coefficient and reducing the electro-osmotic coefficient of the HEM is beneficial for the performance as it helps to supply reactant water to the cathode and hydrate HEM and cathode catalyst layer HEI. In contrast, lower water diffusivity of the cathode catalyst layer HEI helps to retain more reactant water in the high reaction rates region next to the HEM, thus increasing performance. For HEI in vapor cathode without swelling concerns, higher IEC ionomer with increased ionic conductivity is desired. Overall, it is shown how modeling and the results can be used to optimize HEMWE performance.

Acknowledgments

The authors acknowledge the HydroGen Energy Materials Network from the Department of Energy, Hydrogen and Fuel Cell Technologies Office for funding under Contract number DE-AC02-05CH11231.

ORCID

Jiangjin Liu https://orcid.org/0000-0002-1408-4335
Adam Z. Weber https://orcid.org/0000-0002-7749-1624

References

1. M. Yue, H. Lambert, E. Pahon, R. Roche, S. Jemei, and D. Hissel, "Hydrogen energy systems: a critical review of technologies, applications, trends and challenges." *Renew. Sustain. Energy Rev.*, **146**, 111180 (2021).
2. G. W. Crabtree, M. S. Dresselhaus, and M. V. Buchanan, "The hydrogen economy." *Phys. Today*, **57**, 39 (2004).
3. S. Dutta, "A review on production, storage of hydrogen and its utilization as an energy resource." *J. Ind. Eng. Chem.*, **20**, 1148 (2014).
4. P. Nikolaidis and A. Poullikkas, "A comparative overview of hydrogen production processes." *Renew. Sustain. Energy Rev.*, **67**, 597 (2017).
5. J. Armor, "Catalysis and the hydrogen economy." *Catal. Lett.*, **101**, 131 (2005).
6. G. Mulder, J. Hetland, and G. Lenaers, "Towards a sustainable hydrogen economy: Hydrogen pathways and infrastructure." *Int. J. Hydrogen Energy*, **32**, 1324 (2007).
7. A. Kusoglu, "Chalkboard 1-the many colors of hydrogen." *The Electrochemical Society Interface*, **30**, 44 (2021).
8. L. Vidas and R. Castro, "Recent developments on hydrogen production technologies: state-of-the-art review with a focus on green-electrolysis." *Applied Sciences*, **11**, 11363 (2021).
9. A. Ursua, L. M. Gandia, and P. Sanchis, "Hydrogen production from water electrolysis: current status and future trends." *Proc. IEEE*, **100**, 410 (2012).
10. H. A. Miller, K. Bouzek, J. Hnat, S. Loos, C. I. Bernäcker, T. Weißgärber, L. Röntzsch, and J. Meier-Haack, "Green hydrogen from anion exchange membrane water electrolysis: a review of recent developments in critical materials and operating conditions." *Sustainable Energy & Fuels*, **4**, 2114 (2020).
11. I. Vincent and D. Bessarabov, "Low cost hydrogen production by anion exchange membrane electrolysis: a review." *Renew. Sustain. Energy Rev.*, **81**, 1690 (2018).
12. L. Trotochaud, S. L. Young, J. K. Ranney, and S. W. Boettcher, "Nickel–iron oxyhydroxide oxygen-evolution electrocatalysts: the role of intentional and incidental iron incorporation." *JACS*, **136**, 6744 (2014).
13. M. B. Stevens, C. D. Trang, L. J. Enman, J. Deng, and S. W. Boettcher, "Reactive Fe-sites in Ni/Fe (oxy) hydroxide are responsible for exceptional oxygen electrocatalysis activity." *JACS*, **139**, 11361 (2017).
14. J. S. Kim, B. Kim, H. Kim, and K. Kang, "Recent progress on multimetal oxide catalysts for the oxygen evolution reaction." *Adv. Energy Mater.*, **8**, 1702774 (2018).
15. D. Y. Chung, P. P. Lopes, P. F. B. D. Martins, H. He, T. Kawaguchi, P. Zapol, H. You, D. Tripkovic, D. Strmcnik, and Y. Zhu, "Dynamic stability of active sites in hydr (oxy) oxides for the oxygen evolution reaction." *Nat. Energy*, **5**, 222 (2020).
16. A. R. Motz et al., "Performance and durability of anion exchange membrane water electrolyzers using down-selected polymer electrolytes." *J. Mater. Chem. A*, **9**, 22670 (2021).
17. D. Li, A. R. Motz, C. Bae, C. Fujimoto, G. Yang, F. -Y. Zhang, K. E. Ayers, and Y. S. Kim, "Durability of anion exchange membrane water electrolyzers." *Energy Environ. Sci.*, **14**, 3393 (2021).
18. N. Chen, S. Y. Paek, J. Y. Lee, J. H. Park, S. Y. Lee, and Y. M. Lee, "High-performance anion exchange membrane water electrolyzers with a current density of 7.68 A cm^{-2} and a durability of 1000 h." *Energy Environ. Sci.*, **14**, 6338 (2021).
19. X. Luo, D. I. Kushner, J. Li, E. J. Park, Y. S. Kim, and A. Kusoglu, "Anion exchange ionomers: impact of chemistry on thin-film properties." *Adv. Funct. Mater.*, **31**, 2008778 (2021).
20. G. Huang, M. Mandal, N. U. Hassan, K. Groenhout, A. Dobbs, W. E. Mustain, and P. A. Kohl, "Ionomer optimization for water uptake and swelling in anion exchange membrane electrolyzer: oxygen evolution electrode." *J. Electrochem. Soc.*, **167**, 164514 (2020).
21. G. Huang, M. Mandal, N. U. Hassan, K. Groenhout, A. Dobbs, W. E. Mustain, and P. A. Kohl, "Ionomer optimization for water uptake and swelling in anion exchange membrane electrolyzer: hydrogen evolution electrode." *J. Electrochem. Soc.*, **168**, 024503 (2021).
22. F. Xu, Y. Su, and B. Lin, "Progress of alkaline anion exchange membranes for fuel cells: the effects of micro-phase separation." *Frontiers in Materials*, **7**, 4 (2020).
23. S. Gottesfeld, D. R. Dekel, M. Page, C. Bae, Y. Yan, P. Zelenay, and Y. S. Kim, "Anion exchange membrane fuel cells: current status and remaining challenges." *J. Power Sources*, **375**, 170 (2018).
24. N. Chen and Y. M. Lee, "Anion exchange polyelectrolytes for membranes and ionomers." *Prog. Polym. Sci.*, **113**, 101345 (2021).
25. J. Wang et al., "Poly(aryl piperidinium) membranes and ionomers for hydroxide exchange membrane fuel cells." *Nat. Energy*, **4**, 392 (2019).
26. N. Chen et al., "Poly(fluorenyl aryl piperidinium) membranes and ionomers for anion exchange membrane fuel cells." *Nat. Commun.*, **12**, 2367 (2021).
27. L. An, T. S. Zhao, Z. H. Chai, P. Tan, and L. Zeng, "Mathematical modeling of an anion-exchange membrane water electrolyzer for hydrogen production." *Int. J. Hydrogen Energy*, **39**, 19869 (2014).

28. J. Liu, Z. Kang, D. Li, M. Pak, S. M. Alia, C. Fujimoto, G. Bender, Y. S. Kim, and A. Z. Weber, "Elucidating the role of hydroxide electrolyte on anion-exchange-membrane water electrolyzer performance." *J. Electrochem. Soc.*, **168**, 054522 (2021).
29. L. N. Stanislaw, M. R. Gerhardt, and A. Z. Weber, "Modeling electrolyte composition effects on anion-exchange-membrane water electrolyzer performance." *ECS Trans.*, **92**, 767 (2019).
30. J. Zhou, D. Stanier, A. Putz, M. Secanell, and A. Mixed, "Wettability pore size distribution based mathematical model for analyzing two-phase flow in porous electrodes." *J. Electrochem. Soc.*, **164**, F540 (2017).
31. R. B. Bird, E. N. Lightfoot, and W. E. Stewart, *Transport Phenomena* (Wiley, New York, NY) 55, R1 (2002).
32. I. V. Zenyuk, P. K. Das, and A. Z. Weber, "Understanding impacts of catalyst-layer thickness on fuel-cell performance via mathematical modeling." *J. Electrochem. Soc.*, **163**, F691 (2016).
33. L. M. Pant, M. R. Gerhardt, N. Macauley, R. Mukundan, R. L. Borup, and A. Z. Weber, "Along-the-channel modeling and analysis of PEFCs at low stoichiometry: development of a 1+2D model." *Electrochim. Acta*, **326**, 134963 (2019).
34. B. Kientiz, H. Yamada, N. Nonoyama, and A. Z. Weber, "Interfacial water transport effects in proton-exchange membranes." *J. Fuel Cell Sci. Technol.*, **8**, 011013 (2010).
35. Y. Li, T. Zhao, and W. Yang, "Measurements of water uptake and transport properties in anion-exchange membranes." *Int. J. Hydrogen Energy*, **35**, 5656 (2010).
36. H.-S. Shiau, I. V. Zenyuk, and A. Z. Weber, "Elucidating performance limitations in alkaline-exchange-membrane fuel cells." *J. Electrochem. Soc.*, **164**, E3583 (2017).
37. D. Li, E. J. Park, W. Zhu, Q. Shi, Y. Zhou, H. Tian, Y. Lin, A. Serov, B. Zulevi, and E. D. Baca, "Highly quaternized polystyrene ionomers for high performance anion exchange membrane water electrolysers." *Nat. Energy*, 1 (2020).
38. H. Vogt and R. J. Balzer, "The bubble coverage of gas-evolving electrodes in stagnant electrolytes." *Electrochim. Acta*, **50**, 2073 (2005).
39. M. R. Gerhardt, L. M. Pant, J. C. Bui, A. R. Crothers, V. M. Ehlinger, J. C. Fornaciari, J. Liu, and A. Z. Weber, "Methods—practices and pitfalls in voltage breakdown analysis of electrochemical energy-conversion systems." *J. Electrochem. Soc.*, **168**, 074503 (2021).
40. G. A. Lindquist, S. Z. Oener, R. Krivina, A. R. Motz, A. Keane, C. Capuano, K. E. Ayers, and S. W. Boettcher, "Performance and durability of pure-water-fed anion exchange membrane electrolyzers using baseline materials and operation." *ACS Appl. Mater. Interfaces*, **13**, 51917 (2021).
41. A. Kiessling et al., "Influence of supporting electrolyte on hydroxide exchange membrane water electrolysis performance: anolyte." *J. Electrochem. Soc.*, **168**, 084512 (2021).